

Simulation Study on the Mechanism of Intermediate Subdiffusion of Diffusive Particles in Crowded Systems

Meng-Bo Luo* and Dao-Yang Hua

Cite This: *ACS Omega* 2023, 8, 34188–34195

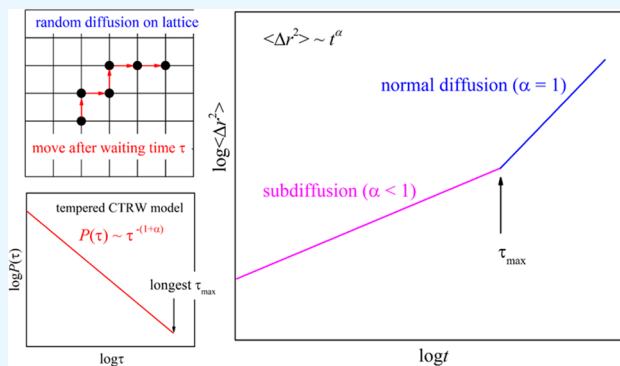
Read Online

ACCESS |

Metrics & More

Article Recommendations

ABSTRACT: The intermediate subdiffusion of diffusive particles in crowded systems is studied for two model systems: the continuous time random walk (CTRW) model and the obstruction-binding model. For the CTRW model with an arbitrarily given longest waiting time τ_{\max} , we find that the diffusive particle exhibits subdiffusion below τ_{\max} and recovers normal diffusion above τ_{\max} . For the obstruction-binding model with randomly distributed attractive obstacles, the diffusion of the diffusive particle is dependent on the binding energy and the density of obstacles. Interestingly, diffusion curves for different binding strengths can be overlapped by rescaling the simulation time, indicating that the diffusive particle in the obstruction-binding model can change from the intermediate subdiffusion to the normal diffusion at a long-term simulation scale. The results of the two model systems show that the diffusive particles only exhibit intermediate subdiffusion below the longest waiting time. Therefore, long timescale subdiffusion would only be observed in the CTRW model with an infinitely long waiting time and in the obstruction-binding model with an infinitely large binding strength.



1. INTRODUCTION

Subdiffusion is a ubiquitous dynamical phenomenon for diffusive particles in crowded systems, characterized by a sublinear increase of the mean-squared displacement (MSD) of the diffusive particle with time t , namely, $\langle \Delta r^2(t) \rangle \sim t^\alpha$, with the diffusion exponent $\alpha < 1$.^{1–3} Subdiffusion is often related to obstructed diffusion in crowded environments with spatial heterogeneity or complex interactions.^{1–9} It was found that the exponent α of trace proteins in a mixed protein solution decreases with the increase of the total protein concentration, clearly demonstrating that the subdiffusion is related to crowding.¹⁰ The subdiffusion of particles in biological systems like living cells and membranes was intensively studied.^{3,11–17} Subdiffusive behavior was observed for the diffusion of trace proteins in living cells crowded with different fillers, such as chromatin, actins, lipid membranes, cytoskeletons, nuclei, and others.^{2,8,10,18,19} It was pointed out that subdiffusion may play an important role in cellular functions, e.g., subdiffusion of particles in the cellular environment increases their probability of finding nearby targets.²⁰ Subdiffusion is also closely linked to drug delivery, the activity of biopolymers in cellular environments, and the functionality of many bio-related devices.²¹ On the other hand, the diffusive property of traces can reflect the surrounding crowded environments. Subdiffusion was also observed for active particles in heterogeneous media with a high enough density of randomly distributed obstacles, and such kind of

motion was believed of prime importance for the survival of most organisms.²²

Subdiffusion of passive particles has received intensive study in physics as well as in biophysics.^{1–9,18,19} A lot of subdiffusive models were introduced to explain the subdiffusive properties of particles in crowded environments with obstacles.^{2,7,12,23–28} There are three main subdiffusion models: the continuous time random walk (CTRW), the fractional Brownian motion (FBM), and the random walk on a fractal structure (RWF). The commonly accepted explanations for the origin of subdiffusion are the geometric constraint and the random attraction of obstacles. Geometric constraints are related to the crowded environment around the diffusing particles.^{2,7,10,23,29–31} Subdiffusive behavior occurs at a high density of obstacles where the molecules are trapped by entropic barriers as the voids are barely interconnected, leading to a stark slowing down of transport and subdiffusive motion.^{7,10} On the other hand, the random attractions between diffusing particles and obstacles not only slows

Received: August 12, 2023

Accepted: August 29, 2023

Published: September 7, 2023



down the diffusion³² but also induces intermittent jumping motion for the diffusing particles.^{33,34} When the attraction is strong enough, subdiffusion could occur at a relatively low density of obstacles or weak entropic barrier.^{34,35} It was found that the diffusion was decreased and subdiffusive behavior appeared when the strength of nonspecific interactions of obstacles within the cytoplasm was increased.³⁵ The stronger the attractive interaction, the more obvious the subdiffusive behavior due to the higher free energy barrier for the diffusion.^{6,36} Spatial heterogeneity is an important factor for subdiffusion. Simulations found that polymers always display normal diffusion in systems with orderly distributed obstacles.³⁷ However, subdiffusion of polymers is exhibited in systems with randomly distributed, attractive obstacles.^{36,38} Randomly distributed, attractive obstacles bring about spatial heterogeneity, which changes the adsorption/desorption behavior of polymers, and polymer chains tend to diffuse toward the places of high obstacle density where the attraction is strong and polymer chains stay there for a long time.^{36,38} To date, the origin of subdiffusion is complex and not well understood. And simple subdiffusion models are not enough to describe the subdiffusive behaviors of tracers in real physical systems due to the complicated conditions.^{19,33}

Subdiffusion of particles, including proteins and polymer chains, in crowded systems was often explained by the CTRW model. The CTRW model is a generalization of a random walk in which the diffusing particle waits for a random waiting time between jumps. The distribution of the waiting time is long-tailed and cannot be averaged, e.g., $P(\tau) \propto \tau^{-(1+\alpha)}$ with $0 < \alpha < 1$. The ergodic breaking due to the heavy tail of the waiting time results in the subdiffusion with the exponent α ($0 < \alpha < 1$) of particles.^{24–26} A typical example is that at each walk the diffusing particle is subject to an exponentially distributed potential V , $P(V) = V_0^{-1} \exp(-V/V_0)$, with $k_B T/V_0 < 1$.²³ Here, k_B is the Boltzmann constant and T is the temperature. Simulations and experiments on the diffusion of polymers in crowded environments with attractive obstacles revealed a heavy long waiting time tail for subdiffusion, although the distribution cannot be expressed exactly by $P(\tau) \sim \tau^{-(1+\alpha)}$, with α the diffusion exponent.^{33,39,40} It was pointed out that the longest waiting time for the polymer chains might be infinite because of the very large binding energy for the adsorbed polymers on attractive obstacles.³⁷ The waiting-time distribution of nonspecific interactions, abundant in the cell, might be nonaverageable and thus the CTRW model is a good microscopic model for one type of anomalous subdiffusion in cells.^{16,33}

However, some experimental and simulation studies on the dynamics of particles in crowded systems showed that the subdiffusion only appeared at an intermediate timescale and then follows a normal diffusion at long timescale. The intermediate subdiffusion can persist for over one or several orders of magnitude timescale. It was found the intermediate subdiffusion of gold-labeled organic molecule in fetal rat skin keratinocyte cells lasted about 2 orders of magnitude timescale and was explained by a finite hierarchy model with different trapped times.^{41,42} An experimental study on the colloidal diffusion over a quenched two-dimensional (2D) random surface also found such an intermediate subdiffusion.³¹ Intermediate subdiffusion was observed in intracellular diffusion of quantum dots by single-particle tracking (SPT) and diffusion of fluorophore-labeled dextran in granular layers by integrative optical imaging (IOI) method.^{43,44} Recently, it

was uncovered that the timescale of the intermediate subdiffusion of nanoparticles in semiflexible networks was also dependent on the rigidity of networks.⁴⁵ On the other hand, it is necessary to temper the broad power-law time distribution because of the finite lifetime of biological particles. For example, a tempered CTRW model using a power-law and exponential decay function was introduced.⁴⁶ Such a system exhibits subdiffusion at short times and eventually a normal diffusion at long times.⁴⁶

It is very interesting to understand what controls the timescale of the intermediate subdiffusion. In this work, to access the transition from subdiffusion to normal diffusion, the distribution of waiting time within the CTRW framework is truncated with a finitely long timescale. Our simulation results show that the timescale for the subdiffusion-normal diffusion transition can be regulated by the longest waiting time, i.e., an intermediate subdiffusion below and a normal diffusion above the longest waiting time. We further study the diffusion of the particle in the obstruction-binding model. For all binding strengths, the particle can change from the intermediate subdiffusion to the normal diffusion at a sufficiently long timescale. We therefore conclude that the diffusive particles only exhibit intermediate subdiffusion below the longest waiting time.

2. MODELS AND SIMULATION METHODS

Simulations on the random diffusion of particles are performed on a 2D square lattice with system size L in both the x and y directions. There are total $S = L^2$ lattice sites. Periodic boundary conditions (PBCs) are employed in the two directions. At the beginning of the simulation, the particle is placed randomly at one lattice site. Then, it moves to one of its four nearest neighbors randomly. We have used three models to study the dynamics of the diffusive particle. To clearly express our results, we use α in the general expression for anomalous subdiffusion, α_{CT} in the expression in the power-law waiting time distribution, and α_{sim} obtained from the simulation results.

2.1. CTRW Model with Quenched Disorders. To simulate quenched disorders,⁴⁷ each lattice site is assigned a fixed waiting time τ in advance. In the simulations, τ is an integer value ranging from 1 to τ_{max} with an integer interval value Δ . Waiting times are assigned a priori for each lattice site randomly with a distribution $P(\tau) \propto \tau^{-(1+\alpha_{CT})}$. For a finite system, $P(\tau)$ is normalized as $P(\tau) = \tau^{-(1+\alpha_{CT})} / \sum_{\tau=1}^{\tau_{max}} \tau^{-(1+\alpha_{CT})}$ for τ ranging from 1 to τ_{max} . As the probability decreases with increasing τ , the longest waiting time τ_{max} is defined as $P(\tau_{max})L^2 \geq M$ and $P(\tau_{max} + \Delta)L^2 < M$, that is, at least one lattice site is assigned τ_{max} . We set $\Delta = 1$ and $M = 1$ in the simulation. Therefore, the longest waiting time τ_{max} increases with increasing system size L but is given in advance. The diffusive particle stays for the assigned waiting time τ on the lattice site before moving to a nearby lattice site. We can also alter Δ to change τ_{max} for a given system size or adjust M to maintain τ_{max} for different system sizes.

2.2. CTRW Model with Annealed Disorders. The diffusive particle moves after an assigned waiting time τ as in the previous model. But τ is not assigned on each lattice in advance of the simulation. Instead, we assign a new waiting time when the diffusive particle moves to other lattice sites. To understand the effect of τ_{max} on the dynamics of particles, the

value of τ_{\max} is arbitrarily given in advance in our simulations. In the simulations, τ is an integer value and is randomly chosen from 1 to τ_{\max} with the distribution $P(\tau) \propto \tau^{-(1+\alpha_{CT})}$. In the simulation, the waiting time τ is obtained through $\tau = r^{-1/\alpha_{CT}}$ with r an evenly distributed random number between 0 and 1. When $\tau > \tau_{\max}$, we discard this value and reproduce a new value. Here, the longest waiting time τ_{\max} is independent of the system size L . Moreover, we can change the value of τ_{\max} artificially in the simulations.

2.3. Obstruction-Binding Model. Immobile obstacles with density $f = n/S$ are randomly placed in the system. Here, n is the number of obstacles. Each obstacle is assigned a binding energy $-\epsilon$ to the adjacent diffusive particle. The diffusive particle can only move to the vacant nearest neighbor lattice sites not occupied by obstacles. At every Monte Carlo step, the diffusive particle tries to move randomly to one of the vacant lattice sites. And the trial move may result in an energy shift ΔE between the binding energy of the new site and that of the original site. The dynamic movement of the diffusive particle obeys the Metropolis algorithm, i.e., the escape probability for the move is set as $p = \exp(-\Delta E/k_B T)$ for the energy shift of the trial move $\Delta E > 0$ or $p = 1$ for $\Delta E \leq 0$. Here, $k_B T$ is set as 1. The situation described by the obstruction-binding model is quite close to the diffusion of polymers in crowded environments.³⁹ The subdiffusion of the obstruction-binding model was studied in the literature.^{42,48} In the present work, we find a new phenomenon when we enlarge the simulation time. The detailed simulation method will be addressed in the next section.

For all three model systems, the MSD of diffusive particles is calculated as

$$\langle \Delta r^2(t) \rangle = \langle |r(t_0 + t) - r(t_0)|^2 \rangle \quad (1)$$

Here, $r(t)$ denotes the position vector of the diffusing particle at time t . Here, t_0 is set as 0. The average is taken over independent samples. In this work, the number of independent samples is 10,000 for these three model systems. However, to complete independent samples, different strategies are used for different model systems. For the CTRW model with quenched disorders, it is a time-consuming process to generate the initial waiting time distribution for all lattice sites, so we use 100 different sets of waiting time distributions and 100 random walks for every set of waiting time distributions. For the CTRW model with annealed disorders, we use 10,000 random walks with different random sequences for the waiting times. Finally, for the obstruction-binding model, we use 10,000 different sets of obstacle configurations and we run one random walk for every set of obstacles. The error of our simulation results is small, so we do not plot the error bar for our simulation results.

The evolution of the MSD of diffusive particles is described by

$$\langle \Delta r^2(t) \rangle \sim t^{\alpha_{\text{sim}}} \quad (2)$$

with α_{sim} a subdiffusion index. The diffusion is denoted as normal diffusion when $\alpha_{\text{sim}} = 1$ and subdiffusion when $\alpha_{\text{sim}} < 1$. The error bar for α_{sim} is less than 0.02.

3. RESULTS AND DISCUSSION

3.1. CTRW Model with Quenched Disorders. Simulations are performed in three systems with sizes $L = 1000$, 10,000, and 20,000. We at first set $\alpha_{CT} = 0.5$, i.e., the

probability of waiting time is $P(\tau) \propto \tau^{-1.5}$. The longest waiting times are about 17,950, 367,400, and 890,000 for systems of size $L = 1000$, 10,000, and 20,000, respectively. Figure 1

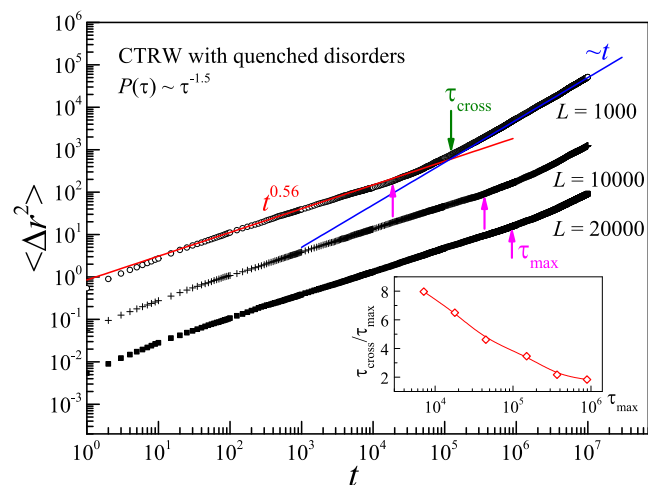


Figure 1. Log–log plot of the mean-squared displacement ($\langle \Delta r^2 \rangle$) versus time t for the diffusing particle in different systems ($L = 1000$, 10,000, and 20,000 from top to bottom) with the probability of waiting time $P(\tau) \propto \tau^{-1.5}$. Curves of $L = 10,000$ and 20,000 are shifted downward by factors of 1/10 and 1/100, respectively. The longest waiting times indicated by magenta arrows are 17,950, 367,400, and 890,000 for the systems of size $L = 1000$, 10,000, and 20,000, respectively. The olive arrow indicates the crossover time τ_{cross} . The red and blue lines have slopes of 0.56 and 1, respectively. The inset shows $\tau_{\text{cross}}/\tau_{\text{max}}$ versus τ_{max} .

presents the log–log evolution of the MSD (Δr^2) with time t for the diffusing particle in these systems. We find a transition from subdiffusion at short times to normal diffusion at long times. The crossover time τ_{cross} for the transition is larger than the longest waiting time τ_{max} . As shown in the inset of Figure 1, we find that $\tau_{\text{cross}}/\tau_{\text{max}}$ decreases gradually with increasing τ_{max} . We expect that it tends to a certain value at sufficiently large τ_{max} . So we expect that the relative difference between the crossover time and τ_{max} becomes smaller with the increase of τ_{max} . Therefore, τ_{max} is used simply for describing the transition from subdiffusion to normal diffusion. The result indicates that the subdiffusion only exists below τ_{max} . Therefore, the simulated subdiffusion exponent α_{sim} is estimated from the slope of the curve below τ_{max} . We find that the exponent α_{sim} is roughly independent of the system size and estimate $\alpha_{\text{sim}} = 0.56$ for $P(\tau) \propto \tau^{-1.5}$. Here, the simulated value $\alpha_{\text{sim}} = 0.56$ is close to the given $\alpha_{CT} = 0.5$ for the distribution of the waiting time.

Based on the three curves shown in Figure 1, the value of $\langle \Delta r^2 \rangle$ above τ_{max} decreases with an increase in the system size L . This is because, in the simulation, we have set a larger τ_{max} for a larger system size. However, if τ_{max} is set the same for different system sizes, values of $\langle \Delta r^2 \rangle$ are the same too. The results suggest that $\langle \Delta r^2 \rangle$ is determined by τ_{max} and not the system size L .

We have also simulated the diffusion of particles for other probability distributions of the waiting time $P(\tau) \propto \tau^{-(1+\alpha_{CT})}$ with different values of α_{CT} in the system of size $L = 10,000$. The longest waiting time τ_{max} decreases with increasing α . Figure 2 presents the simulation results for the given $\alpha_{CT} = 1, 0.9, 0.7$, and 0.5. We again find subdiffusion below τ_{max} even for the case of $\alpha_{CT} = 1$. The variation of α_{sim} with the given α_{CT}

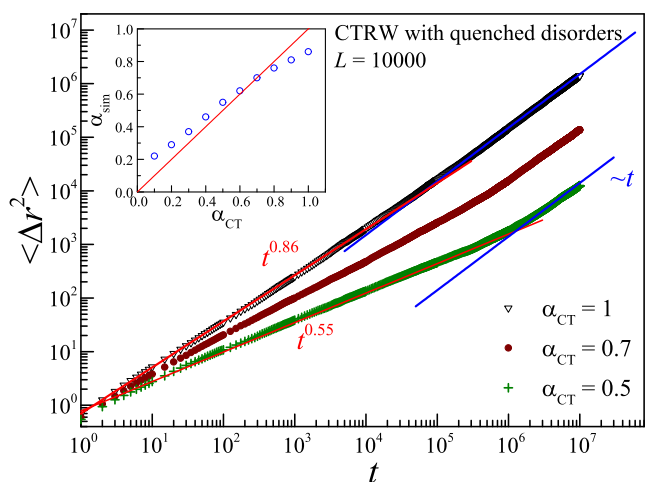


Figure 2. Log–log plot of mean-squared displacement ($\langle \Delta r^2 \rangle$) versus time t for the diffusing particle in systems of different probability distributions of waiting time $P(\tau) \propto \tau^{-(1+\alpha_{CT})}$ with $\alpha_{CT} = 1, 0.7,$ and 0.5 from top to bottom. The blue lines have a slope of 1, while the slopes of the red curves are presented. The inset presents the variation of α_{sim} with given α_{CT} . The straight line shows the relation $\alpha_{sim} = \alpha_{CT}$.

is presented in the inset of Figure 2. We find $\alpha_{sim} \approx \alpha_{CT}$ when α_{CT} is close to 0.6. However, α_{sim} deviates from α_{CT} when α_{CT} is close to 0 or 1. Such a deviation was also observed in simulations on the diffusion of polymer in a crowded system. It was found that the subdiffusion index α_{sim} in MSD curves of polymer chains was different from α_{CT} in probability distributions of the waiting time.^{39,40}

In short, our simulation results show that the intermediate subdiffusion of particles is observed. In the CTRW model with quenched disorders, the given longest waiting time τ_{max} is roughly the crossover time for the transition from subdiffusion to normal diffusion. Therefore, the behavior of particle diffusion will be strongly dependent on the experimental time and the longest waiting time of the system. Subdiffusion will be observed if the duration of the experiment or simulation is shorter than the longest waiting time of the system. On the other hand, we may observe intermediate subdiffusion if the duration is longer than the longest waiting time, while long-time normal diffusion will be observed if the duration is much longer than the longest waiting time. For example, subdiffusion was observed for protein diffusion in a short experimental time and crossover from intermediate subdiffusion to long-time normal diffusion was observed for acetylcholine receptors on membranes in prolonged experiments.^{14,49} For the same reason, long-time subdiffusion was observed for polymer chains in crowded environments due to the long waiting time.⁴⁰

3.2. CTRW Model with Annealed Disorders. Simulations for the CTRW model with annealed disorders are performed in a system of size $L = 10,000$. Figure 3 presents the simulation results of the MSD for three values of $\alpha_{CT} = 0.2, 0.5,$ and 0.8 . Here, we set the longest waiting time $\tau_{max} = 10^9$, longer than the simulation time 10^7 . We find subdiffusive behaviors for all cases. And we find $\alpha_{sim} = \alpha_{CT}$ for $\alpha_{CT} = 0.5$ and α_{sim} deviates from the given value of α_{CT} for $\alpha_{CT} = 0.2$ and 0.8 . The values of α_{sim} are estimated for different values of α_{CT} . The variation of α_{sim} with given α_{CT} is plotted in the inset of Figure 3. We find that the deviation is small for moderate values of α_{CT} from 0.5 to 0.7. However, the deviation becomes

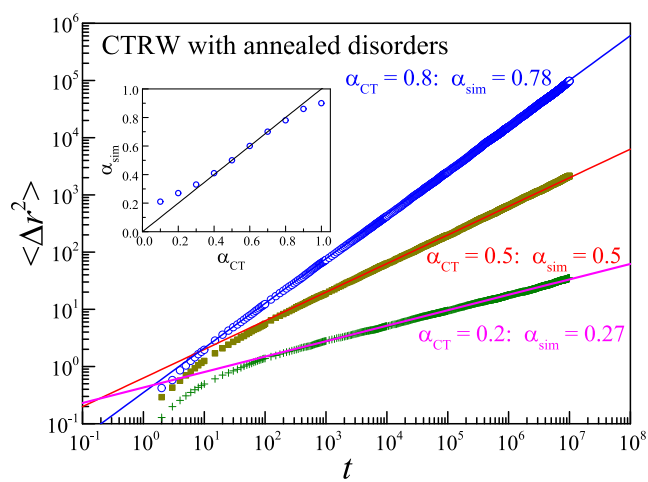


Figure 3. Log–log plot of the mean-squared displacement ($\langle \Delta r^2 \rangle$) versus time t for systems with different distributions of waiting time $P(\tau) \propto \tau^{-(1+\alpha_{CT})}$. From top to bottom, the given exponent α_{CT} is 0.8, 0.5, and 0.2, respectively. The system size $L = 10,000$, and the longest waiting time $\tau_{max} = 10^9$. Solid lines with the slope of values α_{sim} presented in the plot are a guide to the eye. The inset presents the variation of α_{sim} with given α_{CT} . The straight line shows the relation $\alpha_{sim} = \alpha_{CT}$.

a little bigger when α_{CT} is small or large, for example, we have $\alpha_{sim} = 0.21$ for $\alpha_{CT} = 0.1$ and $\alpha_{sim} = 0.9$ for $\alpha_{CT} = 1$.

For the CTRW model with annealed disorders, we have also checked the transition from subdiffusion to normal diffusion by using a smaller τ_{max} in the simulation. Figure 4 shows the

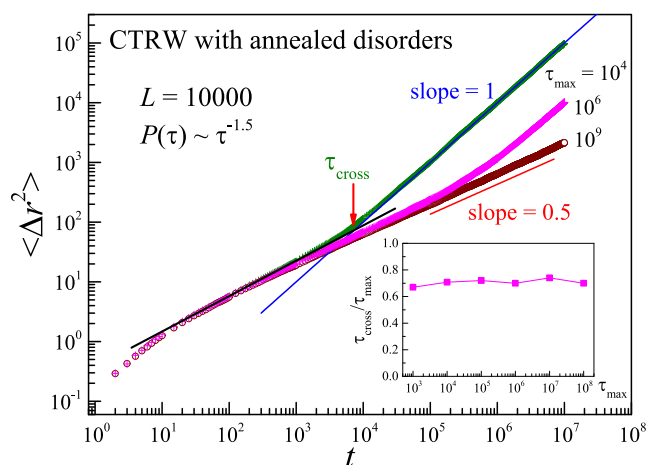


Figure 4. Log–log plot of the mean-squared displacement ($\langle \Delta r^2 \rangle$) versus time t for systems with different longest waiting times τ_{max} ($10^4, 10^6,$ and 10^9 from top to bottom). Solid straight lines with slopes are a guide to the eye. The red arrow indicates the crossover time τ_{cross} . The inset shows τ_{cross}/τ_{max} versus τ_{max} .

results for the distribution $P(\tau) \propto \tau^{-1.5}$ with $\tau_{max} = 10^4, 10^6,$ and 10^8 . Analogous to the results of the CTRW model with quenched disorders, we find a transition from subdiffusion to normal diffusion when the simulation time is longer than τ_{max} . The crossover time τ_{cross} is estimated from the intersection of two straight lines fitting for subdiffusion and normal diffusion, as shown in Figure 4. The values of τ_{cross}/τ_{max} are presented in the inset of Figure 4. For the CTRW model with annealed disorders, we find τ_{cross}/τ_{max} is about 0.7 independent of τ_{max} .

Again, τ_{\max} is used simply for describing the transition from subdiffusion to normal diffusion.

3.3. Obstruction-Binding Model. In the obstruction-binding model, the dynamics of the diffusive particle is affected by the immobile obstacles through the excluded volume and binding energy. The diffusive particle cannot move to the occupied sites by obstacles. When the diffusive particle is at the adjacent site of obstacles, we assign a binding energy $-\varepsilon$ (in the unit of $k_B T$). Here, ε is referred to as the binding strength of obstacles. For the value of the total binding energy E of the particle, there were two simulation models.⁴⁸ One is a uniform binding energy model where the total binding energy is independent of the number of adjacent obstacles, i.e., $E = -\varepsilon$. The other is the variable binding energy model where $E = -n\varepsilon$, with n the number of adjacent obstacles. For example, the total binding energy of the diffusive particle shown in Figure 5 is $E = -\varepsilon$ for the uniform binding energy model, while $E = -2\varepsilon$ for the variable binding energy model. The variable binding energy model is used in the present work.

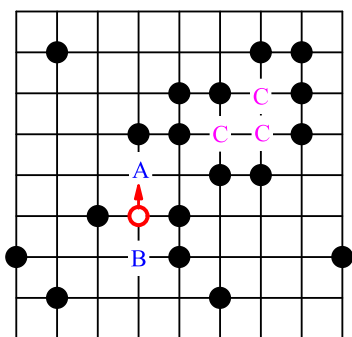


Figure 5. Sketch of the simulation system with immobile obstacles (black solid circles) and a diffusive particle (red open circle). The diffusive particle can move to vacant sites A or B. Vacant sites marked by “C” are closed areas, and they are forbidden for the initial position of the diffusive particle.

The diffusive particle can move to nearby vacancies. Figure 5 shows a sketch of the system where obstacles (black circles) are immobile. The dynamic move of the diffusive particle (red circle) obeys the Metropolis algorithm, i.e., the escape probability for the move is set as $W = \exp(-\Delta E/k_B T)$, with ΔE the energy increment for the move. For both the uniform binding energy and variable binding energy models, intermediate subdiffusion and long-timescale normal diffusion were discovered.⁴⁸ It was pointed out that the diffusion is anomalous in the obstruction-binding model with a non-Gaussian distribution of binding times.⁵ Moreover, the equilibrium of initial condition on the dynamics of the diffusive particle was examined.⁴⁸ It was found that the system with random initial conditions (without equilibrium) exhibits more obvious intermediate subdiffusion and has a lower diffusion exponent than that with thermal equilibrium initial conditions.⁴⁸ After thermal equilibrium, the diffusive particle has a larger probability to locate at a lower energy position.

In the present work, we use Metropolis dynamics for the dynamics of the diffusive particle. For every move, the binding energies E_{old} and E_{new} before and after the particle's move, respectively, are calculated. The energy increment $\Delta E = E_{\text{new}} - E_{\text{old}}$ can be expressed as $\Delta E = -(n_{\text{new}} - n_{\text{old}})\varepsilon$, with n_{old} and n_{new} the numbers of adjacent obstacles before and after the particle's move, respectively. The diffusive particle is placed

randomly on one of the vacant sites on the surface. However, closed areas as shown in Figure 5 are not allowed for the initial position of the diffusive particle.

The MSD of the diffusive particle is calculated after the system is equilibrated with time t_{eq} . The time unit is Monte Carlo step (MCS) where the particle is tried to move once in one MCS. Figure 6a presents the evolution of MSD for

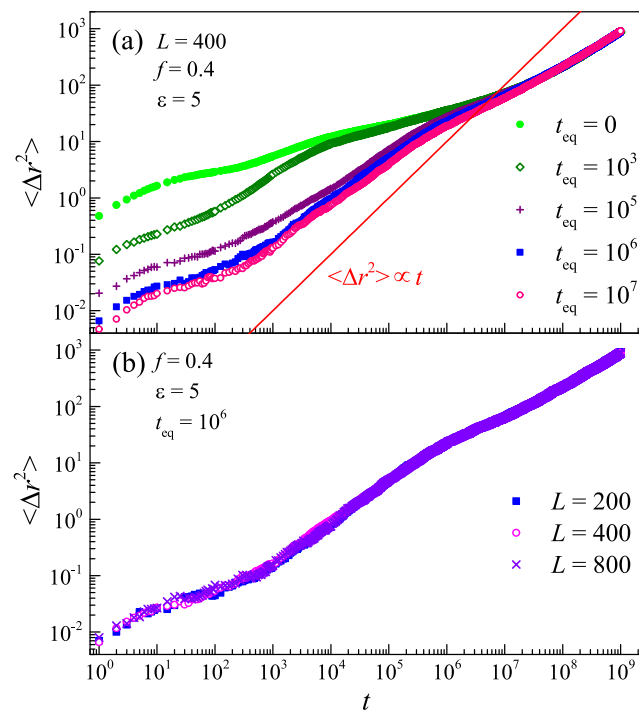


Figure 6. Log–log plot of the mean-squared displacement of particle ($\langle \Delta r^2 \rangle$) versus time t for systems with different equilibration time t_{eq} (a) and with different sizes L (b). The obstacle density is $f = 0.4$, the binding strength is $\varepsilon = 5$, and the equilibration time is $t_{\text{eq}} = 10^6$. The straight line in (a) has a slope of 1.

different t_{eq} values for the system with binding strength $\varepsilon = 5$. MSD decreases with increasing t_{eq} in the short timescale, consistent with the results of the uniform as well as variable binding energy models.⁴⁸ The particle will locate at low-energy sites after equilibrium, so the particle moves slowly after equilibrium. However, MSD almost does not change with t_{eq} when t_{eq} reaches 10^6 . As it is easy to equilibrate a system with low ε , we here set $t_{\text{eq}} = 10^6$ for other ε . We have also checked the system size effect on the evolution of MSD. Figure 6b shows the evolution of MSD for three system sizes $L = 200, 400$, and 800 . We find the results are roughly independent of the system size. Therefore, we use the system of size $L = 400$ in our simulations.

Figure 7 shows the evolution of MSD for different obstacle densities f for the system with binding strength $\varepsilon = 5$. For small $f = 0.05$ and 0.1 , we find normal diffusion with $\langle \Delta r^2 \rangle \propto t$ at a large timescale $t > 10^8$. From the results of CTRW, the results indicate that the longest waiting time τ_{\max} is about 10^8 for small f . However, for large $f = 0.3$ and 0.4 , we do not observe normal diffusion for the longest simulation time, implying that the longest waiting time τ_{\max} increases with f . We have checked the state of the diffusive particle. The state is defined as the number of adjacent obstacles, n . Since $\varepsilon = 5$ is large, we find the most probable state of the particle is $n = 2$, for instance, we

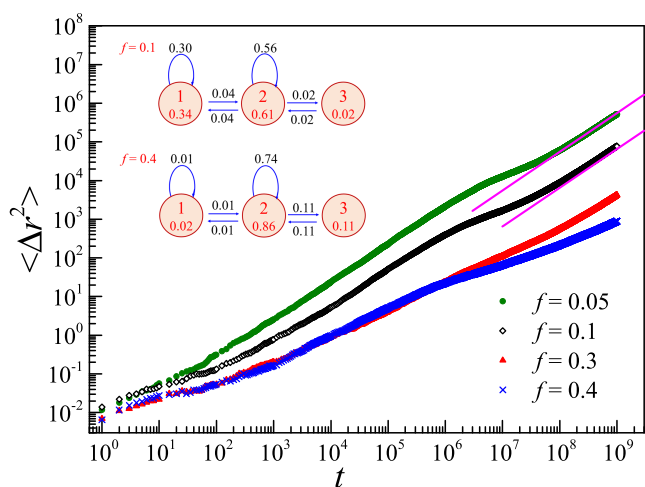


Figure 7. Log–log plot of the mean-squared displacement $\langle \Delta r^2 \rangle$ versus time t for systems with different obstacle densities $f = 0.05, 0.1, 0.3,$ and 0.4 . System size $L = 400$, obstacle-binding strength $\varepsilon = 5$, and equilibration time $t_{\text{eq}} = 10^6$. Straight lines have a slope of 1. The inset shows some of the most important state transfer probabilities for $f = 0.1$ and 0.4 . The integer and digit in circles indicate the state of the particle and the corresponding probability. While the digit near the arrows shows the state transfer probability.

have $p(2) = 0.61$ and 0.86 for $f = 0.1$ and 0.4 , respectively. The diffusion of particles is accompanied by a change of state. So we have calculated the transfer probability for the diffusive particle. The inset of Figure 7 shows some of the most important state transfer probabilities for $f = 0.1$ and 0.4 . For $f = 0.4$, the diffusive particle is mostly trapped in the state with $n = 2$, so the diffusion is small. While for $f = 0.1$, there is a relatively large transfer probability between states $n = 1$ and 2 . Thus, the diffusion of the particle at a small f is large.

The inset of Figure 8 presents the MSD $\langle \Delta r^2 \rangle$ versus time t for systems with different binding energies. Here, the system

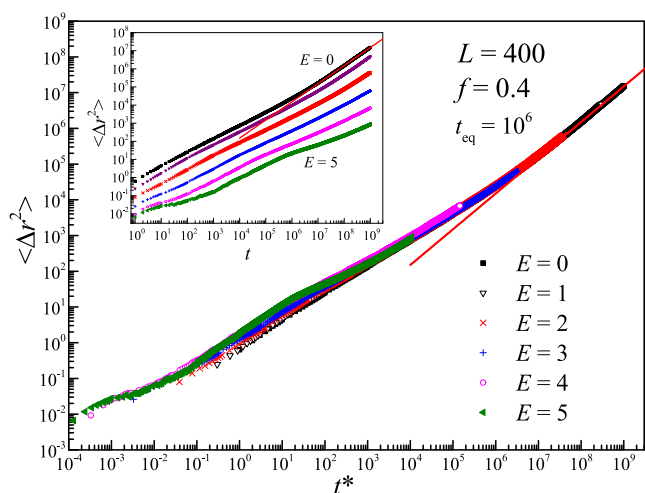


Figure 8. Log–log plot of the mean-squared displacement $\langle \Delta r^2 \rangle$ versus rescaled time $t^* = tC_1 t^{-\beta}$ for systems with different binding strengths ε . Values of pre-factor C_1 and exponent β are $(0.3, 0.0)$, $(0.039, 0.0)$, $(0.0033, 0.0)$, $(0.00033, 0.04)$, $(0.00013, 0.12)$ for $\varepsilon = 1, 2, 3, 4,$ and 5 , respectively. The inset presents $\langle \Delta r^2 \rangle$ versus the simulation time t for $\varepsilon = 0, 1, 2, 3, 4,$ and 5 from top to bottom. System size $L = 400$, obstacle density $f = 0.4$, and equilibration time $t_{\text{eq}} = 10^6$.

with $\varepsilon = 0$ means only the excluded volume effect of obstacles is considered. We find normal diffusion in the simulation time region since $f = 0.4$ is lower than the percolation point. Analogous to the $\varepsilon = 0$ case, we also find normal diffusion for the system with a small ε ($\varepsilon = 1$ and 2) in the simulation time region. The reason is that the longest waiting time τ_{max} is small at small ε . With the increase of ε , the longest waiting time τ_{max} increases. When τ_{max} is larger than the simulation time, the system always shows subdiffusion in the simulation time region, as those curves of $\varepsilon > 3$. However, all of the MSD curves are similar for different ε values. Therefore, it is possible to switch from subdiffusion to normal diffusion over an even longer simulation time. Thus, we have tried to overlap these MSD curves by rescaling these MSD curves.

According to the theory of CTRW, the number of diffusion steps grows with time as $n(t) \approx At^\alpha$.⁵⁰ So we scale the simulation time t to $t^* = tf(t) = tC_1 t^{-\beta}$ for $\varepsilon > 0$. By properly choosing pre-factor C_1 and exponent β for every ε , we find different curves can collapse into one main curve. As shown in Figure 8, we thus conclude that all of the systems could exhibit normal diffusion at large t^* . The results thus suggest that the diffusive particle in the obstacle-binding model will always show normal diffusion at a sufficiently long timescale. This is in agreement with the diffusion of colloid particles on a 2D random surface where subdiffusion was observed only at an intermediate timescale.³¹ Also, long-time normal diffusion was observed for particles diffusing among larger attractive crowding spheres.⁵¹ On the other hand, we find that C_1 decreases while β increases with increasing the binding energy, indicating that the diffusion of particles becomes slow at strong binding.

The normal diffusion behavior of the obstruction-binding model can be understood from the distribution of waiting time for the particle jumping to a nearby site. The jump probability equals the escape probability $p = \exp(-\Delta E/k_B T)$ if the energy increment for the jump $\Delta E > 0$. In the obstruction-binding model, ΔE can be $\varepsilon, 2\varepsilon,$ or 3ε . For each ΔE , the distribution of waiting time $\tau = k$ satisfies geometric distribution, $P(\tau = k) = (1 - p)^{k-1} p$, with $p = \exp(-\Delta E/k_B T)$. The mean waiting time of the geometric distribution is finite as $\langle \tau \rangle = 1/p = \exp(\Delta E/k_B T)$, which is different from the infinitely large mean waiting time for CTRW. Therefore, we will always find the normal diffusion behavior at a long timescale for the obstruction-binding model.

4. CONCLUSIONS

The intermediate subdiffusion of diffusive particles in crowded systems is studied for two model systems: the continuous time random walk (CTRW) model and the obstruction-binding model. For the CTRW model, by introducing arbitrarily the longest waiting time τ_{max} , we find the diffusive particle exhibits subdiffusion below τ_{max} and recovers normal diffusion above τ_{max} . Therefore, for the real CTRW model with an infinitely large τ_{max} , a long-timescale subdiffusion will be found. In the obstruction-binding model with randomly distributed attractive obstacles, the diffusion is dependent on the binding energy and density of obstacles. Interestingly, we find different diffusive curves for different binding energies can be overlapped by rescaling the simulation time. The result implies that the diffusive particle in the obstruction-binding model can change from the intermediate subdiffusion to the normal diffusion at a long-term simulation scale. However, the timescale increases with increasing binding energy; thus, the

intermediate subdiffusion will last a long time window at a large binding energy.

AUTHOR INFORMATION

Corresponding Author

Meng-Bo Luo – School of Physics, Zhejiang University, Hangzhou 310027, China; orcid.org/0000-0002-0783-0352; Email: luomengbo@zju.edu.cn

Author

Dao-Yang Hua – School of Physics, Zhejiang University, Hangzhou 310027, China

Complete contact information is available at:

<https://pubs.acs.org/10.1021/acsomega.3c05945>

Notes

The authors declare no competing financial interest.

ACKNOWLEDGMENTS

This work was supported by the National Natural Science Foundation of China under grant no. 11974305 and by the Open Research Fund Program of Key Laboratory of Surface & Interface Science of Polymer Materials of Zhejiang Province (SISPM-2022-06).

REFERENCES

- (1) Bouchaud, J.-P.; Georges, A. Anomalous diffusion in disordered media: Statistical mechanisms, models and physical applications. *Phys. Rep.* **1990**, *195*, 127–293.
- (2) Barkai, E.; Garini, Y.; Metzler, R. Strange kinetics of single molecules in living cells. *Phys. Today* **2012**, *65*, 29–35.
- (3) Krapf, D. Mechanisms Underlying Anomalous Diffusion in the Plasma Membrane. In *Current Topics in Membranes*; Elsevier, 2015; Vol. 75, pp 167–207.
- (4) Saxton, M. J. Anomalous diffusion due to obstacles: A Monte Carlo study. *Biophys. J.* **1994**, *66*, 394–401.
- (5) Dix, J. A.; Verkman, A. S. Crowding effects on diffusion in solutions and cells. *Annu. Rev. Biophys.* **2008**, *37*, 247–263.
- (6) Sokolov, I. M. Models of anomalous diffusion in crowded environments. *Soft Matter* **2012**, *8*, 9043–9052.
- (7) Höfling, F.; Franosch, T. Anomalous transport in the crowded world of biological cells. *Rep. Prog. Phys.* **2013**, *76*, No. 046602.
- (8) Metzler, R.; Jeon, J.-H.; Cherstvy, A. G.; Barkai, E. Anomalous diffusion models and their properties: non-stationarity, non-ergodicity, and ageing at the centenary of single particle tracking. *Phys. Chem. Chem. Phys.* **2014**, *16*, 24128–24164.
- (9) Niu, Q.; Wang, D. *Curr. Opin. Colloid Interface Sci.* **2019**, *39*, 162–172.
- (10) Weiss, M.; Elsner, M.; Kartberg, F.; Nilsson, T. Anomalous subdiffusion is a measure for cytoplasmic crowding in living cells. *Biophys. J.* **2004**, *87*, 3518–3524.
- (11) Banks, D. S.; Fradin, C. Anomalous diffusion of proteins due to molecular crowding. *Biophys. J.* **2005**, *89*, 2960–2971.
- (12) Jeon, J. H.; Tejedor, V.; Burov, S.; Barkai, E.; Selhuber-Unkel, C.; Berg-Sørensen, K.; Oddershede, L.; Metzler, R. In vivo anomalous diffusion and weak ergodicity breaking of lipid granules. *Phys. Rev. Lett.* **2011**, *106*, No. 048103.
- (13) Di Rienzo, C.; Piazza, V.; Gratton, E.; Beltram, F.; Cardarelli, F. Probing short-range protein Brownian motion in the cytoplasm of living cells. *Nat. Commun.* **2014**, *5*, No. 5891.
- (14) Metzler, R.; Jeon, J.-H.; Cherstvy, A. G. Non-Brownian diffusion in lipid membranes: Experiments and simulations. *Biochim. Biophys. Acta, Biomembr.* **2016**, *1858*, 2451–2467.
- (15) Lampo, T. J.; Stylianidou, S.; Backlund, M. P.; Wiggins, P. A.; Spakowitz, A. J. Cytoplasmic RNA-protein particles exhibit non-gaussian subdiffusive behavior. *Biophys. J.* **2017**, *112*, 532–542.
- (16) Woringner, M.; Izeddin, I.; Favard, C.; Berry, H. Anomalous subdiffusion in living cells: Bridging the gap between experiments and realistic models through collaborative challenges. *Front. Phys.* **2020**, *8*, No. 134.
- (17) Goychuk, I.; Pöschel, T. Fingerprints of viscoelastic subdiffusion in random environments: Revisiting some experimental data and their interpretations. *Phys. Rev. E* **2021**, *104*, No. 034125.
- (18) Metzler, R.; Klafter, J. The random walk's guide to anomalous diffusion: A fractional dynamics approach. *Phys. Rep.* **2000**, *339*, 1–77.
- (19) Meroz, Y.; Sokolov, I. M. A toolbox for determining subdiffusive mechanisms. *Phys. Rep.* **2015**, *573*, 1–29.
- (20) Guigas, G.; Weiss, M. Sampling the cell with anomalous diffusion - The discovery of slowness. *Biophys. J.* **2008**, *94*, 90–94.
- (21) Lin, C.-C.; Parrish, E.; Composto, R. J. Macromolecule and particle dynamics in confined media. *Macromolecules* **2016**, *49*, 5755–5772.
- (22) Chepizhko, O.; Peruani, F. Diffusion, subdiffusion, and trapping of active particles in heterogeneous media. *Phys. Rev. Lett.* **2015**, *111*, No. 160604.
- (23) Ben-Avraham, D.; Havlin, S. *Diffusion and Reactions in Fractals and Disordered Systems*; Cambridge university press: Cambridge, 2000.
- (24) Scher, H.; Montroll, E. W. Anomalous transit-time dispersion in amorphous solids. *Phys. Rev. B* **1975**, *12*, 2455–2477.
- (25) Frauenfelder, H.; Sligar, S. G.; Wolynes, P. G. The energy landscapes and motions of proteins. *Science* **1991**, *254*, 1598–1603.
- (26) Weigel, A. V.; Simon, B.; Tamkun, M. M.; Krapf, D. Ergodic and nonergodic processes coexist in the plasma membrane as observed by single-molecule tracking. *Proc. Natl. Acad. Sci. U.S.A.* **2011**, *108*, 6438–6443.
- (27) Mandelbrot, B. B.; van Ness, J. W. Fractional Brownian motions, fractional noises and applications. *SIAM Rev.* **1968**, *10*, 422–437.
- (28) Bronstein, I.; Israel, Y.; Kepten, E.; Mai, S.; Shav-Tal, Y.; Barkai, E.; Garini, Y. Transient anomalous diffusion of telomeres in the nucleus of mammalian cells. *Phys. Rev. Lett.* **2009**, *103*, No. 018102.
- (29) Sentjabrskaja, T.; Zaccarelli, E.; de Michele, C.; Sciortino, F.; Tartaglia, P.; Voigtmann, T.; Egelhaaf, S. U.; Laurati, M. Anomalous dynamics of intruders in a crowded environment of mobile obstacles. *Nat. Commun.* **2016**, *7*, No. 11133.
- (30) Krasowska, M.; Strzelewiec, A.; Dudek, G.; Cieřła, M. Structure-diffusion relationship of polymer membranes with different texture. *Phys. Rev. E* **2017**, *95*, No. 012155.
- (31) Su, Y.; Ma, X.; Lai, P.-Y.; Tong, P. Colloidal diffusion over a quenched two-dimensional random potential. *Soft Matter* **2017**, *13*, 4773–4785.
- (32) Sorichetti, V.; Hugouvieux, V.; Kob, W. Structure and dynamics of a polymer-nanoparticle composite: Effect of nanoparticle size and volume fraction. *Macromolecules* **2018**, *51*, 5375–5391.
- (33) Wang, D.; He, C.; Stoykovich, M. P.; Schwartz, D. K. Nanoscale topography influences polymer surface diffusion. *ACS Nano* **2015**, *9*, 1656–1664.
- (34) Cai, S.; Liu, J.; Tian, M.; Wang, K.; Shen, L. Diffusion dynamics of a single collapsed homopolymer globule at the solid-liquid interface. *Soft Matter* **2020**, *16*, 2431–2436.
- (35) Etoc, F.; Balloul, E.; Vicario, C.; Normanno, D.; Liře, D.; Sittner, A.; Piehler, J.; Dahan, M.; Coppey, M. Non-specific interactions govern cytosolic diffusion of nanosized objects in mammalian cells. *Nat. Mater.* **2018**, *17*, 740–746.
- (36) Li, C. Y.; Luo, M. B.; Huang, J. H.; Li, H. Equilibrium and dynamical properties of polymer chains in random medium filled with randomly distributed nano-sized fillers. *Phys. Chem. Chem. Phys.* **2015**, *17*, 31877–31886.
- (37) Huang, X. W.; Peng, Y.; Huang, J. H.; Luo, M. B. A study on the diffusivity of polymers in crowded environments with periodically distributed nanoparticles. *Phys. Chem. Chem. Phys.* **2017**, *19*, 29975–29983.

(38) Tsehay, D. A.; Luo, M. B. Static and dynamic properties of a semiflexible polymer in a crowded environment with randomly distributed immobile nanoparticles. *Phys. Chem. Chem. Phys.* **2018**, *20*, 9582–9590.

(39) Lu, R. X.; Huang, J. H.; Luo, M. B. A simulation study on the subdiffusion of polymer chains in crowded environments containing nanonparticles. *Phys. Chem. Chem. Phys.* **2022**, *24*, 3078–3085.

(40) Hua, D. Y.; Khan, R. A. A.; Luo, M. B. Langevin Dynamics Simulation on the Diffusivity of Polymers in Crowded Environments with Immobile Nanoparticles. *Macromolecules* **2022**, *55*, 10468–10478.

(41) Murase, K.; Fujiwara, T.; Umemura, Y.; Suzuki, K.; Iino, R.; Yamashita, H.; Saito, M.; Murakoshi, H.; Ritchie, K.; Kusumi, A. Ultrafine membrane compartments for molecular diffusion as revealed by single molecule techniques. *Biophys. J.* **2004**, *86*, 4075–4093.

(42) Saxton, M. J. A biological interpretation of transient anomalous subdiffusion. I. Qualitative model. *Biophys. J.* **2007**, *92*, 1178–1191.

(43) Li, H.; Dou, S. X.; Liu, Y. R.; Li, W.; Xie, P.; Wang, W. C.; Wang, P. Y. Mapping intracellular diffusion distribution using single quantum dot tracking: Compartmentalized diffusion defined by endoplasmic reticulum. *J. Am. Chem. Soc.* **2015**, *137*, 436–444.

(44) Xiao, F.; Hrabe, J.; Hrabetova, S. Anomalous extracellular diffusion in rat cerebellum. *Biophys. J.* **2015**, *108*, 2384–2395.

(45) Xu, Z.; Dai, X.; Bu, X.; Yang, Y.; Zhang, X.; Man, X.; Zhang, X.; Doi, M.; Yan, L. T. Enhanced heterogeneous diffusion of nanoparticles in semiflexible networks. *ACS Nano* **2021**, *15*, 4608–4616.

(46) Fa, K. S. Continuous-time random walk: Crossover from anomalous regime to normal regime. *Phys. Rev. E* **2010**, *82*, No. 012101.

(47) Tateishi, A. A.; Ribeiro, H. V.; Sandev, T.; Petreska, I.; Lenzi, E. K. Quenched and annealed disorder mechanisms in comb models with fractional operators. *Phys. Rev. E* **2020**, *101*, No. 022135.

(48) Saxton, M. J. Anomalous diffusion due to binding: A Monte Carlo study. *Biophys. J.* **1996**, *70*, 1250–1262.

(49) He, W.; Song, H.; Su, Y.; Geng, L.; Ackerson, B. J.; Peng, H. B.; Tong, P. Dynamic heterogeneity and non-Gaussian statistics for acetylcholine receptors on live cell membrane. *Nat. Commun.* **2016**, *7*, No. 11701.

(50) Lubelski, A.; Sokolov, I. M.; Klafter, J. Nonergodicity mimics inhomogeneity in single particle tracking. *Phys. Rev. Lett.* **2008**, *100*, No. 250602.

(51) Putzel, G. G.; Tagliazucchi, M.; Szeleifer, I. Diffusion of particles among larger attractive crowding spheres. *Phys. Rev. Lett.* **2014**, *113*, No. 138302.